

SYMMETRIES OF THE ROTATING MEAN FIELD*

S. FRAUENDORF

Department of Physics, University of Notre Dame, Notre Dame, IN 46556, USA
andInstitute for Nuclear and Hadronic Physics, Research Center Rossendorf
PB 51 01 19, 01314 Dresden, Germany*(Received July 18, 2001)*

The discrete symmetries of the rotating mean field lead to a variety of rotational bands with different sequences of spin and parity. We focus on the breaking of chiral symmetry in rotating triaxial nuclei.

PACS numbers: 21.10.-k, 23.20.Lv, 25.70.Gh, 27.60+j

1. Introduction

Chirality appears in molecules composed of more than four different atoms and is typical for the biomolecules. The simplest examples are molecules like $\text{CH}_3\text{CH}_2\text{-C}\equiv\text{IHCH}_3$ (2-iodobutene). It contains a stereocenter, which is the C atom to which four different groups are attached (the bonds are explicitly indicated). The three groups I, H, and CH_3 and the bond to CH_3CH_2 form a left-handed or a right-handed screw. These two “enantiomers” are related to each other by a mirror reflection.

In chemistry chirality is of static nature because it characterizes the geometrical arrangement of the atoms. Particle physics is the other field where chirality is encountered. Here it has a dynamical character, since it distinguishes between the parallel and antiparallel orientation of the spin with respect to the momentum of massless fermions. The neutrino, which appears only as left-handed specie, is an example. Frauendorf and Meng [1] recently pointed out that the rotation of triaxial nuclei may attain a chiral character. The lower panel of Fig. 1 illustrates this new possibility. We denote the three principal axes (PA) of triaxial density distribution by l , i , and s , which stand for long, intermediate and short, respectively. The

* Invited talk presented at the *High Spin Physics 2001* NATO Advanced Research Workshop, dedicated to the memory of Zdzisław Szymański, Warsaw, Poland, February 6–10, 2001.

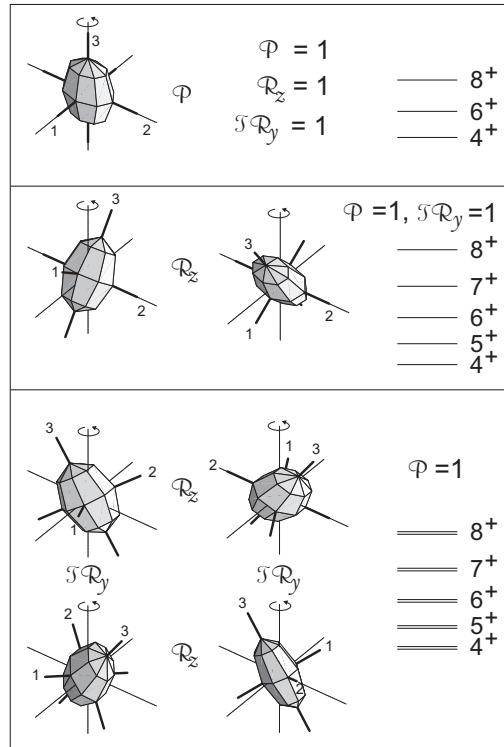


Fig. 1. The discrete symmetries of the mean field of a rotating triaxial reflection symmetric nucleus (three mirror planes). The axis of rotation (z) is marked by the circular arrow. It coincides with the angular momentum \vec{J} . The structure of the rotational bands associated with each symmetry type is illustrated on the right side. The meaning of the symmetry operations is explained in Section 4. Note the change of chirality induced by $\mathcal{TR}_y(\pi)$ in the lowest panel. The axes s, i, l are denoted by 1, 2, 3, respectively.

angular momentum vector \vec{J} introduces chirality by selecting one of the octants. In four of the octants the axes $l, i,$ and s form a left-handed and in the other four a right-handed system. This gives rise to two degenerate rotational bands because all octants are energetically equivalent. Hence the chirality of nuclear rotation results from a combination of dynamics (the angular momentum) and geometry (the triaxial shape).

If we speak about the “symmetry of a molecule” we mean the symmetry of the “intrinsic” wavefunction, which describes the electrons and the relative positions of the nuclei. The total wavefunction, which additionally includes the orientation of the whole molecule in space, represents the symmetry of the Hamiltonian, which is invariant under 3D rotations and space inversion.

This higher symmetry leads to characteristic restrictions in the rotational spectrum, as for example shown in Fig. 1. This argument must be modified for nuclei, because the nucleons are not on fixed positions. The rotating mean field takes the role of the molecular intrinsic wavefunction. It is described by the cranking model, which most generally consists in applying the mean field approximation (Hartree-Fock or related procedures) to the two-body Routhian

$$H' = H - \omega J_z, \quad (1)$$

where H is the two-body Hamiltonian of the nucleus and J_z is the angular momentum component on the z -axis, which we choose as the axis of rotation. The mean field solution $|\rangle$ has in general a lower symmetry than implied by the Routhian (1). In such a case one speaks of “spontaneous symmetry breaking”. The loss of rotational symmetry with respect to the z -axis leads to rotational spectra. Like in the case of molecules, the presence or absence of discrete symmetries (finite rotations, space inversion and time reversal) of (1) in $|\rangle$ leads to characteristic rotational spectra, examples of which are shown in Fig. 1. In Section 4 we give a more systematic discussion.

2. Tilted Axis Cranking

The cranking model describes the uniform classic rotation of the mean field solution $|\rangle$. Our symmetry argument is based on the presumption that the axis of uniform rotation needs not to agree with one of the PA of the density distribution. This does not hold for a rigid triaxial body, like a molecule for example, which can uniformly rotate only about the l - and s -axes. However, already Rieman [2] pointed out that a liquid may uniformly rotate about an axis tilted with respect to the PA, if there is an intrinsic vortical motion. In the case of the nucleus the quantization of the angular momentum of the nucleons at the Fermi surface generates the vorticity which enables rotation about a tilted axis.

The semiclassical mean field description of tilted nuclear rotation was developed in [3–5]. In the following we shall refer to it as the Tilted Axis Cranking (TAC) approach [5]. Figure 1 illustrates the different symmetries if the mean field is assumed to be reflection symmetric. In the upper panel the axis of rotation (which is chosen to be z) coincides with one of the PA, *i.e.* the finite rotation $\mathcal{R}_z(\pi) = 1$. This symmetry implies the signature quantum number α , which restricts the total angular momentum to the values $I = \alpha + 2n$, with n integer ($\Delta I = 2$ band) [6]. In the middle panel the rotational axis lies in one of the planes spanned by two PA (planar tilt). Since then $\mathcal{R}_z(\pi) \neq 1$, there is no longer a restriction of the values I can take. The band is a sequence of states the I of which differ by 1 ($\Delta I = 1$ band). There is a second symmetry in the upper two panels: The rotation

$\mathcal{R}_y(\pi)$ transforms the density into an identical position but changes the sign of the angular momentum vector \vec{J} . Since the latter is odd under the time reversal operation \mathcal{T} , the combination $\mathcal{T}\mathcal{R}_y(\pi) = 1$.

In the lower panel the axis of rotation is out of the three planes spanned by the PA. The operation $\mathcal{T}\mathcal{R}_y(\pi) \neq 1$. It changes the chirality of the axes l , i and s with respect to the axis of rotation \vec{J} . Since the left- and the right-handed solutions have the same energy, they give rise to two degenerate $\Delta I = 1$ bands. They are the even ($|+\rangle$) and odd ($|-\rangle$) linear combinations of the two chiralities, which restore the spontaneously broken $\mathcal{T}\mathcal{R}_y(\pi)$ symmetry.

Figure 2 illustrates how such a solution may arise. The proton aligns its angular momentum \vec{j}_p with the short axis of the density distribution. This orientation maximizes the overlap of its orbital with the triaxial density, which corresponds to minimal energy, because the core-particle interaction is attractive. The neutron hole aligns its angular momentum \vec{j}_h with the long axis. This orientation minimizes the overlap of its orbital with the triaxial density, which corresponds to minimal energy, because the core-hole interaction is repulsive. The angular momentum of the core \vec{R} is of collective nature. It likes to orient along the intermediate axis, which has the largest moment of inertia, because the density distribution deviates strongest from rotational symmetry with respect to this axis.

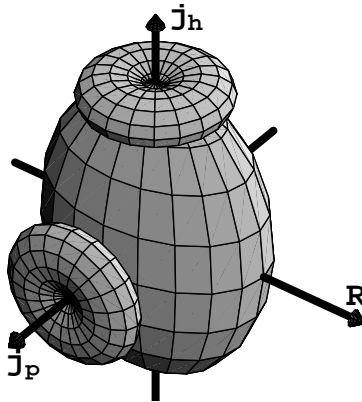


Fig. 2. Orbitals of a high- j proton and a high- j neutron hole coupled to the triaxial density distribution.

The structure shown in Fig. 2 was first suggested by Frisk and Bengtsson [4] for the configuration $[\pi g_{9/2}, \nu g_{9/2}^{-1}]$ in ${}_{39}^{84}\text{Y}_{45}$ assuming a triaxial shape with $\gamma = 30^\circ$. A later study [8] showed that this nucleus is indeed axial, which is consistent with the absence of a chiral doublet band in this nucleus.

TABLE I

Chirality in the mass 134 region. TAC calculations: P — planar solution, S — chiral solution in a short I interval, and L — chiral solution in a long I interval. Observation of chiral doubling: CR — chiral rotation (the two $\Delta I = 1$ bands come very close), CV — chiral vibration (the two $\Delta I = 1$ bands remain separated). From [7, 8].

$Z \backslash N$	67	68	69	70	71	72	73	74	75	76	77	78
65												
64												
63									S CV			
62												
61									L CR			
60									L	L	L	
59			P AC				CV		L CR		CV	
58										L		
57							CV		M CV		CV	
56						P AC						
55							CV		S CV		CV	
54												
53												

Dimitrov, Frauendorf and Dönau [8] found the first completely self-consistent chiral solution for $^{134}_{59}\text{Pr}_{75}$ with the maximal triaxiality of $\gamma \approx 30^\circ$. Figure 3 shows that in this nucleus one observes that two $\Delta I = 1$ bands, which are based on the $[\pi h_{11/2}, \nu h_{11/2}^{-1}]$ configuration, merge forming a doublet structure [9]. Consistent with the experiment, the TAC solution attains chiral character only for $I > 15$. Table I gives an overview over the existing TAC calculations and the experimental evidence for chirality in the neighbourhood of ^{134}Pr . The study is yet incomplete. However, it seems that there is an island of chirality around $Z = 59$ and $N = 75$. In the $N = 75$ chain, the shores have probably been reached at $Z = 63$ and 55. Figure 3 shows some of the observed chiral pairs. For most cases there remains a splitting of few 100 keV between the partners. They are listed as Chiral Vibrators (CV) in Table I.

The cases, when the two partners merge are listed as Chiral Rotors (CR). TAC solutions that are chiral only in a short I interval are observed as vibrators and the solutions that are chiral in a more extended interval are seen as rotors. Note that there are also chiral solutions for $Z = 60$. They correspond to a combination of the $[\pi h_{11/2}, \nu h_{11/2}^{-1}]$ configuration with a proton in a low spin state ($N = 75$ and 77). For $N = 76$ there is an additional neutron in a low spin state.

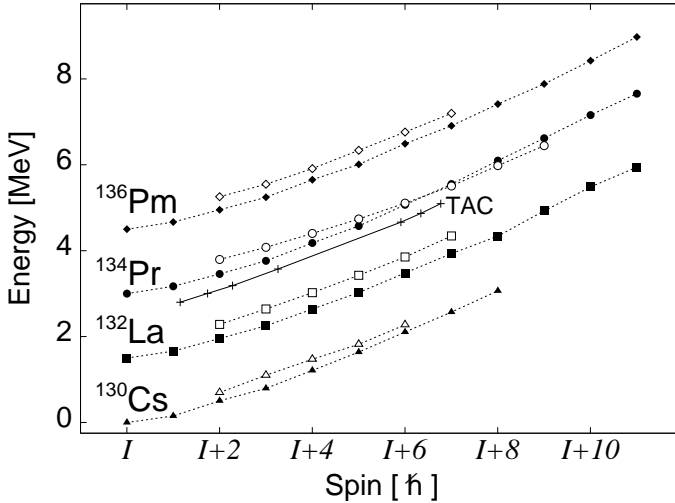


Fig. 3. Chiral sister bands in the $N = 75$ isotones based on the configuration $\pi h_{11/2} \nu h_{11/2}^{-1}$. The parity of the bands is $+$ and $I = 9$. From [7]. The TAC calculation from [8] is included.

TAC calculations [8, 10] predict other regions, where chirality can be expected:

- Around ^{188}Ir . The active high- j orbitals are $h_{9/2}$ or $i_{13/2}$ protons combined with $i_{13/2}$ neutron holes.
- Around ^{106}Ru . The active high- j orbitals are $g_{9/2}$ proton holes combined with $h_{11/2}$ neutrons.
- Around ^{79}Br . The active high- j orbitals are $g_{9/2}$ protons combined with $g_{9/2}$ neutron holes.

In the latter two cases the TAC calculations do not give genuine minima in the chiral sector but a valley along which the energy does not depend on the orientation of the rotational axis. These nuclei will probably show soft chiral vibrational excitations. For ^{136}Nd a chiral solution was found at $I > 34$, which combines a *pair* of $h_{11/2}$ combined with a *pair* of $h_{11/2}$ neutron holes [10]. The larger angular momenta of the particles and holes imply a larger angular momentum of the core. One may expect that the larger angular momenta reduce the tunneling between the left- and right-handed solutions and the chiral partners come very close together.

3. Dynamics — particle rotor calculations

TAC permits us to find the static chiral mean-field solutions, from which one can obtain the energies and electro-magnetic transition probabilities under the assumption *that the tunneling is negligible* between the left- and right-handed solutions (see [8,11]). The experimental candidates for chirality found so far show an energetic splitting between sister bands, which indicates substantial tunneling. The dynamics of the orientation of \vec{J} has been studied for the model case of a proton particle and a neutron hole coupled to a triaxial rotor with maximal asymmetry ($\gamma = 30^\circ$) and the irrotational flow relation $\mathcal{J}_l = \mathcal{J}_s = \mathcal{J}_i/4$ between the moments of inertia [1,12,13].

Figure 4 shows the result of such calculations. At the beginning of the lowest band the angular momentum originates from the particle and the hole, whose individual angular momenta are aligned with the s - and l -axes. These orientations correspond to a maximal overlap of the particle and hole densities with the triaxial potential, as illustrated in Fig. 2. A $\Delta I = 1$ band is generated by adding the rotor momentum \vec{R} in the s - l plane (planar tilt).

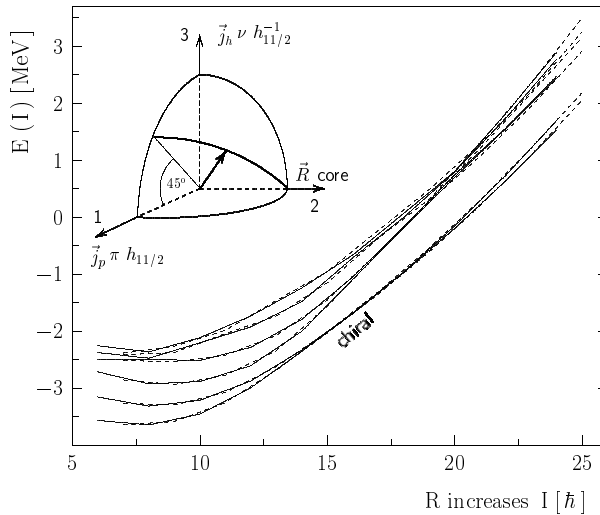


Fig. 4. Rotational levels of $h_{11/2}$ particles and holes coupled to a triaxial rotor with $\gamma = 30^\circ$. Full lines: $\alpha = 0$ (even I). Dashed lines: $\alpha = 1$ (odd I). The insets show the orientation of the angular momentum with respect to the triaxial potential, where 1, 2 and 3 correspond to the short, intermediate and long principal axes, respectively. The angular momentum vector moves along the heavy arcs. The position displayed corresponds to the spin interval $13 < I < 18$, where the two lowest bands are nearly degenerate. The right-handed position is shown. The left-handed is obtained by reflection through the 1-3 plane. From [1].

There is a second $\Delta I = 1$ band representing a vibration of \vec{J} out of the s - l plane, which is generated by a wobbling of \vec{R} . This is a more precise description of the chiral vibration mentioned above. Higher in the band, \vec{R} reorients towards the i -axis, which has the maximal moment of inertia. The left- and the right-handed positions of \vec{J} separate. Since they couple only by some tunneling, the two bands come very close together in energy. This is the regime we called chiral rotation. The reorientation of \vec{R} , *i.e.* the transition from chiral vibration to rotation is well localized in the spectrum Fig. 4. It appears also in the higher bands at larger I . The transition is signalized by a marked change of the M1 transition: The $B(\text{M1})$ values between the chiral vibrational bands are small as compared to the intra band values. The $B(\text{M1})$ values between the sister bands of chiral rotors are comparable with the intra band values.

4. Broken reflection symmetry

Let us discuss the discrete symmetries more systematically. The two-body Routhian (1) is invariant with respect to

1. $\mathcal{R}_z(\psi)$, rotation about the z -axis,
2. \mathcal{P} , space inversion,
3. $\mathcal{R}_z(\pi)$, rotation about the z -axis by an angle of π ,
4. $\mathcal{TR}_y(\pi)$, rotation about the y -axis by an angle of π combined with the time reversal \mathcal{T} .

The symmetry (4) is a consequence of \vec{J} being odd under the time reversal operation \mathcal{T} . Since we discuss rotational bands, we assume that 1 is broken. The symmetry operations 2-4 are two-fold and commute. Table II lists the different combinations by which the rotating mean field can break the three symmetries.

In the preceding sections the case of a reflection symmetric mean field was considered. In addition to the three symmetries illustrated in Fig. 1, there are two more (IV and V) mentioned in Table II. It is not clear if they exist in nuclei. If the restriction to reflection symmetry is lifted many new discrete symmetries arise. Let us start by assuming that the mean field has no discrete symmetry at all. There is no restriction of I by $\mathcal{R}_z(\pi)$. The operations \mathcal{P} , and $\mathcal{TR}_y(\pi)$, which leave the two-body Routhian invariant, define four nonequivalent degenerate mean field solutions $|\rangle$, $|\mathcal{P}\rangle$, $|\mathcal{TR}_y(\pi)\rangle$, and $|\mathcal{PTR}_y(\pi)\rangle$. This means that the bands appear as four fold degenerate $\Delta I = 1$ sequences. For each value of I , there are two levels of positive and two levels of negative parity. The cases when symmetries reduce this

TABLE II

Discrete symmetries of the rotating mean field. Columns 2–4 list the result of the symmetry operation. D(ifferent) means the mean field has changed and S(ame) it has not. An operation as entry means it is identical with the one of the column. Columns 5 shows the spin and parity I^π of the rotational states, where I^\pm means that there are two degenerate states of opposite parity (parity doubling). The 2 indicates that there are two degenerate states with the same I^π (chiral doubling) and $2I^\pm$ means that there are four degenerate states, two with I^+ and two with I^- (parity and chiral doubling). For I–V also $\pi = -$ appears, although it is not explicitly indicated. From [11].

type	\mathcal{P}	$\mathcal{R}_z(\pi)$	$\mathcal{TR}_y(\pi)$	level sequence
I	S	S	S	$I^+, (I+2)^+, (I+4)^+, \dots$
II	S	D	S	$I^+, (I+1)^+, (I+2)^+, \dots$
III	S	D	D	$2I^+, 2(I+1)^+, 2(I+2)^+, \dots$
IV	S	S	D	$2I^+, 2(I+2)^+, 2(I+4)^+, \dots$
V	S	D	$\mathcal{R}_z(\pi)$	$I^+, (I+1)^+, (I+2)^+, \dots$
VI	D	S	S	$I^\pm, (I+2)^\pm, (I+4)^\pm, \dots$
VII	D	D	S	$I^\pm, (I+1)^\pm, (I+2)^\pm, \dots$
VIII	D	S	D	$2I^\pm, 2(I+2)^\pm, 2(I+4)^\pm, \dots$
IX	D	D	$\mathcal{R}_z(\pi)$	$I^\pm, (I+1)^\pm, (I+2)^\pm, \dots$
X	$\mathcal{R}_z(\pi)$	D	S	$I^+, (I+1)^-, (I+2)^+, \dots$
XI	$\mathcal{R}_z(\pi)$	D	D	$2I^+, 2(I+1)^-, 2(I+2)^+, \dots$
XII	$\mathcal{TR}_y(\pi)$	S	D	$I^\pm, (I+2)^\pm, (I+4)^\pm, \dots$
XIII	$\mathcal{TR}_y(\pi)$	D	D	$I^\pm, (I+1)^\pm, (I+2)^\pm, \dots$
XIV	$\mathcal{R}_z(\pi)$	D	$\mathcal{R}_z(\pi)$	$I^+, (I+1)^-, (I+2)^+, \dots$
XV	D	D	D	$2I^\pm, 2(I+1)^\pm, 2(I+2)^\pm, \dots$

degeneracy are summarized in Table II. Figs. 5 and 6 illustrate the cases, which can be visualized by combining the angular momentum vector \vec{J} with the density distribution.

Figure 5 shows the symmetry types when the density distribution has two mirror planes. In the middle panel the rotational axis lies perpendicular to one of the mirror planes (X in Table II), which contains the important special case of axial symmetry with the axis of rotation perpendicular to the symmetry axis. The symmetry $\mathcal{TR}_y(\pi) = 1$ ensures that there is only one state for a given parity and $\mathcal{S} = \mathcal{PR}_z(\pi) = 1$ defines the simplex quantum

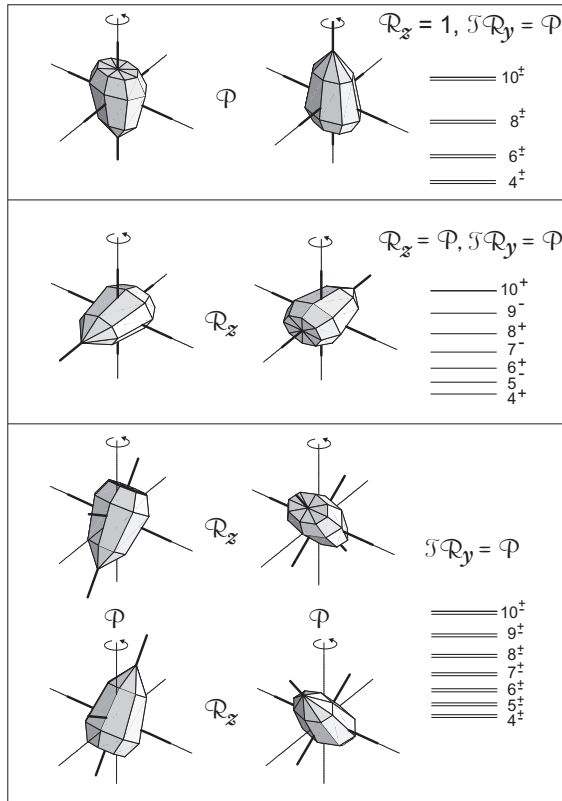


Fig. 5. The discrete symmetries of the mean field of a rotating nucleus with two mirror planes. Cf. caption of Fig. 1. From [11].

number σ , which fixes the parity for a given spin I , as $\pi = (-)^{I-\sigma}$ [14,15]. This symmetry is well known in the light actinides (see *e.g.* [11,16]).

In the lower panel of Fig. 5 the rotational axis lies in one of the two mirror planes but is not perpendicular to the other plane (VII). Since the simplex is no longer a good quantum number, the parity is not fixed by the spin any more. There is a parity doublet for each spin I . Some evidence for this symmetry exists in the light actinides (see *e.g.* [11,16]).

Ref. [17] recently classified the mean field solutions according to the discrete symmetries, which arise from the combination of $\mathcal{R}_x(\pi)$, $\mathcal{R}_y(\pi)$, $\mathcal{R}_z(\pi)$, $\mathcal{TR}_x(\pi)$, $\mathcal{TR}_y(\pi)$, $\mathcal{TR}_z(\pi)$ and \mathcal{T} . The symmetries listed in Table II are special cases of their scheme. Since their remaining symmetries do not leave the two-body Routhian invariant, they are not relevant for the discussion of spontaneous symmetry breaking in rapidly rotating nuclei.

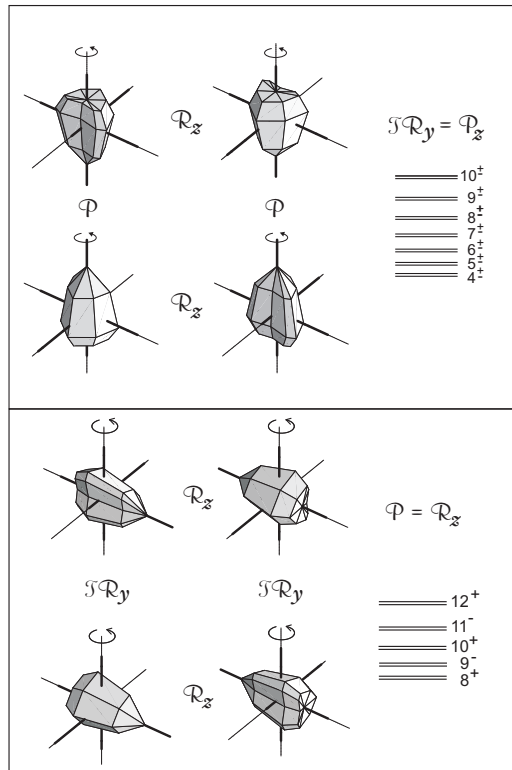


Fig. 6. Discrete symmetries of the mean field of a rotating nucleus with one mirror plane. *Cf.* caption of Fig. 1. From [11].

5. Conclusions

The cranking model, which provides uniformly rotating mean field solutions, is the standard microscopic description of high spin states. The existence and structure of rotational bands reflects the symmetries of these solutions. The relation between angular momentum \vec{J} and velocity $\vec{\omega}$ is much more complex than for molecules or liquids, because nuclei are composed of nucleons on orbits with an angular momentum, which is largely controlled by quantization. As a consequence, the axis for uniform rotation (the angular momentum vector \vec{J}) can take any direction with respect to the density distribution.

The combination of \vec{J} with the density distribution gives rise to a variety of discrete symmetries. A new possibility is the breaking of chiral symmetry in triaxial reflection symmetric nuclei. It shows up as a pair of identical

$\Delta I = 1$ bands of the same parity. Mean field solutions of this type have been found in nuclides around $A = 134$, where there is experimental evidence for a small island of chirality. The existence of chiral sister bands is also predicted for other mass regions.

There are 15 different discrete symmetries of the rotating mean field if time odd components are considered and no reflection asymmetry is demanded. Some of them have a spin-parity sequence that is distinctly different from the familiar ones, which would be a clear experimental signature of the symmetry. So far there is only evidence for the symmetries leading to the spin parity sequences: $I^+, (I + 2)^+, (I + 4)^+, \dots$ (good signature), $I^+, (I + 1)^+, (I + 2)^+, \dots$ (tilted rotation), $2I^+, 2(I + 1)^+, 2(I + 2)^+, \dots$ (chiral doubling), $I^+, (I + 1)^-, (I + 2)^+, \dots$ (good simplex), and $I^\pm, (I + 1)^\pm, (I + 2)^\pm, \dots$ (parity doubling).

Support by the grant DE-FG02-95ER40934 is acknowledged.

REFERENCES

- [1] S. Frauendorf, J. Meng, *Nucl. Phys.* **A617**, 131 (1997).
- [2] B. Riemann, *Abh. Kön. Ges. Wiss., Göttingen* **9**, 1 (1860).
- [3] A.K. Kerman, N. Onishi, *Nucl. Phys.* **A361**, 179 (1981).
- [4] H. Frisk, R. Bengtsson, *Phys. Lett.* **196B**, 14 (1987).
- [5] S. Frauendorf, *Nucl. Phys.* **A557**, 259c (1993).
- [6] R. Bengtsson, S. Frauendorf, *Nucl. Phys.* **A327**, 139 (1979).
- [7] K. Starosta *et al.*, *Phys. Rev. Lett.* **86**, 971 (2001).
- [8] V.I. Dimitrov, S. Frauendorf, F. Döna, *Phys. Rev. Lett.* **84**, 5732 (2000).
- [9] C. Petrache *et al.*, *Nucl. Phys.* **A597**, 106 (1996).
- [10] V. Dimitrov, S. Frauendorf, to be published.
- [11] S. Frauendorf, *Rev. Mod. Phys.* **73**, 463 (2001).
- [12] K. Starosta *et al.*, *Nucl. Phys.* **A682**, 375c (2001).
- [13] R.A. Bark *et al.* *Nucl. Phys.* **A691**, 577 (2001).
- [14] S. Frauendorf, V.V. Pashkevich, *Phys. Lett.* **B141**, 23 (1984).
- [15] W. Nazarewicz *et al.*, *Phys. Rev. Lett.* **52**, 1272 (1984); **53**, 2060 (1984) (E).
- [16] P.A. Butler, W. Nazarewicz, *Rev. Mod. Phys.* **68**, 349 (1996).
- [17] J. Dobaczewski *et al.*, *Phys. Rev.* **C62**, 014311 (2000); **C62**, 014310, (2000).